

The normal state scattering rate in high- T_c cuprates

N.E. Hussey

H. H. Wills Physics Laboratory, University of Bristol, Bristol, BS8 1TL, United Kingdom.

(October 28, 2018)

I present a new phenomenological model for the normal state transport properties of high- T_c cuprates. In particular, I identify a form of scattering rate that may account, qualitatively and quantitatively, for the normal state (magneto)-transport properties of $\text{Tl}_2\text{Ba}_2\text{CuO}_{6+\delta}$ and $\text{Bi}_2\text{Sr}_2\text{CaCu}_2\text{O}_{8+\delta}$ from optimal doping through to the overdoped side of the phase diagram. The form of the scattering rate is also consistent with features seen in photoemission spectroscopy in $\text{Bi}_2\text{Sr}_2\text{CaCu}_2\text{O}_{8+\delta}$ and offers a new intuitive way to understand the evolution of the temperature dependence of the inverse Hall angle with disorder and with carrier concentration.

PACS numbers: 72.10.-d, 74.25.Fy, 74.72.Fq

I. INTRODUCTION

The search for a consistent description for the anomalous normal state transport properties of high- T_c cuprates (HTC) has been a long and fascinating journey. Many phenomenological models seeking to identify the appropriate form for the normal state scattering rate have been offered but none have captured the complete picture. From the very beginning, it was clear that the T -linear behavior of the in-plane resistivity ρ_{ab} , extending over an anomalously broad range of temperature for optimally doped (OP) cuprates, would be difficult to reconcile within a conventional Fermi-liquid (FL) framework.¹ Later observations of the T^2 dependence and impurity dependence of the inverse Hall angle $\cot\Theta_H$,² together with the modified Kohler's rule (in-plane orbital magnetoresistance (MR) $\Delta\rho_{ab}/\rho_{ab} \sim \tan^2\Theta_H$),³ seemed to constitute an insurmountable challenge to FL theory.

Several notable attempts to explain the anomalous transport behavior of HTC within a modified FL scenario followed, each one incorporating a particular form for the (strong) anisotropy of the transport scattering rate within the plane arising out of some form of coupling to a singular bosonic mode; be it spin fluctuations,^{4,5} charge fluctuations⁶ or d -wave superconducting fluctuations.⁷ In each case, however, inconsistencies with certain aspects of the experimental data were exposed.

Given these failings, other more exotic models, based on a non-FL ground state, gained prominence within the community; most notably the two-lifetime picture of Anderson⁸ and the Marginal-Fermi-liquid (MFL) model of Varma and co-workers.^{9,10} The two-lifetime model has been extremely insightful for understanding the experimental situation in OP cuprates, but has yet to provide an explanation for the results of Angle-Resolved Photoemission Spectroscopy (ARPES) nor the evolution of the transport phenomena across the HTC phase diagram. The MFL hypothesis assumes that optimum T_c lies in proximity to a quantum critical point and consequently, quasi-particles are ill defined everywhere on the Fermi surface with a self-energy that is governed simply by the temperature scale. In contrast to the two-lifetime picture, this model is consistent with certain aspects of

ARPES measurements,¹¹ though not all. Most notably, the recently reported evidence of a kink in the energy dispersion¹² seems at odds with a scenario based on quantum criticality. Yet again, predictions of the MFL theory have so far been confined to optimum doping.

In this paper, I propose a new model for the normal state scattering rate that offers an alternative route to understanding the HTC phenomenology. The salient features of the model are presented in section II. The model has as its basis, two novel but physically reasonable assumptions. Firstly, the dominant scattering rate is assumed to vary as T^2 everywhere on the Fermi surface, but in contrast to previous approaches, both the elastic *and* the inelastic parts of the self-energy contain strong (doping dependent) basal plane anisotropy. The second key assumption is that this anisotropic scattering rate eventually saturates (on different regions of the Fermi surface at different temperatures) at a value equivalent to the Mott-Ioffe-Regel criterion for coherent band transport. In section III A, the model is compared with experimental data on $\text{Tl}_2\text{Ba}_2\text{CuO}_{6+\delta}$ (Tl2201) at different doping concentrations. Excellent qualitative and quantitative agreement is found between the model and experimental data for $\rho_{ab}(T)$, $\cot\Theta_H(T)$ and significantly, the magnitude and T -dependence of $\Delta\rho_{ab}/\rho_{ab}(T)$, with relatively few fitting parameters. The model goes beyond previous proposals in that it can also account for the evolution of the observed normal state behavior across the overdoped (OD) region of the phase diagram from optimum doping. In section III B, the model is applied to recent ARPES measurements of the quasi-particle scattering rate and normal state transport data for $\text{Bi}_2\text{Sr}_2\text{CaCu}_2\text{O}_{8+\delta}$ (Bi2212) and comparisons are made with the single-layer $\text{Bi}_2\text{Sr}_{2-x}\text{La}_x\text{CuO}_{6+\delta}$ (Bi2201). In particular, the model is shown to provide a natural explanation for the non-universal power law behavior of $\cot\Theta_H(T)$ observed in the Bi-based cuprates.^{13,14} Finally, in section IV, justification arguments for this particular choice of scattering rate are presented and the implications of this phenomenological model for the physics of HTC across the phase diagram are discussed, with suggestions for future study. In the process, I challenge two of the previously established paradigms of the normal

state in HTC; namely the linear low- T behavior of $\rho_{ab}(T)$ and the relevance of the non-saturating $\rho_{ab}(T)$ observed at higher temperatures.

II. MODEL

There is strong experimental evidence from both ARPES¹⁵ and c -axis MR¹⁶ that the dominant scattering mechanism in HTC is highly anisotropic within the basal plane, being strongest at the so-called ‘anti-nodal’ points at $(\pi, 0)$ and weakest at the ‘nodal’ points (π, π) . In an anisotropic 2D metal, Ong has shown that the Hall angle $\tan\Theta_H(T)$ will be dominated by those regions of the Fermi surface where the scattering is weakest.¹⁷ If the anisotropy is sufficiently high, $\cot\Theta_H(T)$ should therefore reflect the T -dependence of the scattering rate at the nodal points. Given that in the majority of cuprates, $\cot\Theta_H(T) \sim A + BT^2$, I take this to represent the intrinsic T -dependence of the dominant scattering rate in HTC. A key stipulation of the present model is that the scattering rate has this same T -dependence *everywhere* on the Fermi surface, but has four-fold symmetry, being maximum along $(\pi, 0)$.^{15,16} Combined with an elastic scattering rate $\Gamma_0(\phi)$, which may also contain 4-fold anisotropy,¹⁰ the ‘ideal’ scattering rate $\Gamma_{\text{ideal}}(\phi)$ is written as

$$\Gamma_{\text{ideal}}(\phi, T) = \Gamma_0(\phi) + \Gamma_T(\phi, T)$$

where

$$\Gamma_0(\phi) = \alpha(1 + c \cos^2 2\phi)$$

and the T -dependent scattering rate

$$\Gamma_T(\phi, T) = \beta(1 + e \cos^4 2\phi)T^2$$

Here ϕ represents the angle between the in-plane Fermi wave vector and $(k_x, 0)$ whilst c and e are the anisotropy factors for the impurity and T -dependent scattering rates respectively. The coefficients α and β can be roughly estimated from Hall angle measurements. The particular angular dependencies for $\Gamma_0(\phi)$ and $\Gamma_T(\phi)$ shown above are chosen to reflect the four-fold symmetry of $\Gamma_{\text{ideal}}(\phi)$ and to be consistent with ARPES measurements, as outlined in section III B. $\Gamma_{\text{ideal}}(\phi)$ is largest ($= \alpha(1 + c) + \beta(1 + e)T^2$) along $(\pi, 0)$ and smallest, but still finite ($= \alpha + \beta T^2$), along (π, π) .

The second key feature of the model is the application of the Mott-Ioffe-Regel (MIR) limit to HTC. In its basic form, the MIR criterion states that the quasi-particle mean free path ℓ cannot become smaller than the lattice spacing a , since at this point, the quasi-particles lose their coherence and conventional Boltzmann transport analysis becomes irrelevant. When k -dependence is introduced, different regions of the Fermi surface become incoherent at different temperatures. Likewise, the scattering rate at different points on the Fermi surface will saturate (at the MIR limit) at different temperatures.

The first evidence for resistivity saturation in metals, consistent with the MIR limit, was reported in the A-15 superconductors.¹⁸ The T -dependence of the resistivity was found to fit extremely well to a simple ‘parallel-resistor’ model,¹⁹ suggesting that the ideal resistivity (i.e. in the absence of saturation) was somehow shunted by a large saturation resistivity ρ_{max} corresponding to $\ell = a$. Using the MIR criterion as his guide, Gurvitch later argued²⁰ that there must be a minimum time below which no scattering event can take place, i.e. a minimum distance a over which each carrier gains additional drift velocity before being scattered, and from this derived an elegant understanding of the appropriateness of the parallel-resistor model for resistivity saturation.

In the spirit of Gurvitch’s picture, I introduce for HTC a maximum scattering rate (minimum lifetime) $\Gamma_{\text{max}}(\phi)$, equivalent to $\ell = a$, and define an *effective* scattering rate $\Gamma_{\text{eff}}(\phi, T)$ at each point on the Fermi surface of the parallel-resistor form, i.e.

$$\frac{1}{\Gamma_{\text{eff}}(\phi, T)} = \frac{1}{\Gamma_{\text{ideal}}(\phi, T)} + \frac{1}{\Gamma_{\text{max}}(\phi)}$$

$\Gamma_{\text{eff}}(\phi, T)$ is then inserted into the Jones-Zener expansion of the standard Boltzmann transport equation for a quasi-2D Fermi surface to extract all measurable transport coefficients. A derivation of the appropriate expressions is included as an Appendix. Since the Fermi velocity v_F ($= 1 - 3 \times 10^5 \text{ ms}^{-1}$) has already been determined by ARPES, the value of Γ_{max} can be fixed directly by the MIR criterion ($\ell = a$) giving Γ_{max} in the range 250 - 750 THz (150 - 450 meV). As will be shown, this derivation of $\Gamma_{\text{eff}}(\phi, T)$ is sufficient to explain the many unusual T -dependencies that appear in the normal state transport in HTC.

The T -dependencies of $\Gamma_{\text{eff}}(\phi, T)$ for the two momentum directions $(\pi, 0)$ and (π, π) are illustrated schematically in Fig. 1. For concreteness, the parameters used in this simulation are those appropriate for OP Tl2201, namely $\alpha = 18 \text{ meV}$, $\beta = 1.15 \times 10^{-3} \text{ meV/K}^2$, $c = 6$, $e = 30$ and $\Gamma_{\text{max}}^{(\pi,0)} = 435 \text{ meV}$. Along $(\pi, 0)$, $\Gamma_{\text{ideal}}(T)$ reaches Γ_{max} at $T_c \sim 90\text{K}$, at which point, the anti-nodal quasi-particles will become incoherent. Due to the presence of the ‘shunt’ Γ_{max} , however, $\Gamma_{\text{eff}}(T)$ is always smaller than $\Gamma_{\text{ideal}}(T)$ and approaches saturation much more gradually. For the quasi-particles at (π, π) on the other hand, $\Gamma_{\text{ideal}}(T)$ reaches Γ_{max} at a much higher temperature ($T \sim 600\text{K}$). Hence, at the nodal points, well-defined coherent quasi-particles exist at all relevant temperatures. Note that $\Gamma_{\text{eff}}(T)$ at (π, π) is quasi-linear over a wide temperature range. The ‘effective’ anisotropy factor e^* ($= \Gamma_{\text{eff}}^{(\pi,0)} / \Gamma_{\text{eff}}^{(\pi,\pi)} - 1$) is significantly lower than e for all finite T , reaching a maximum value ~ 7 at the temperature where $\Gamma_{\text{ideal}}^{(\pi,0)}$ first crosses Γ_{max} (see inset to Fig. 1). The overall effect is a transport scattering rate $\Gamma_{\text{eff}}(\phi, T)$ whose anisotropy initially grows with increasing T but then gradually becomes more isotropic at higher temperatures as the scattering rate at different regions of the Fermi surface tends towards saturation. In

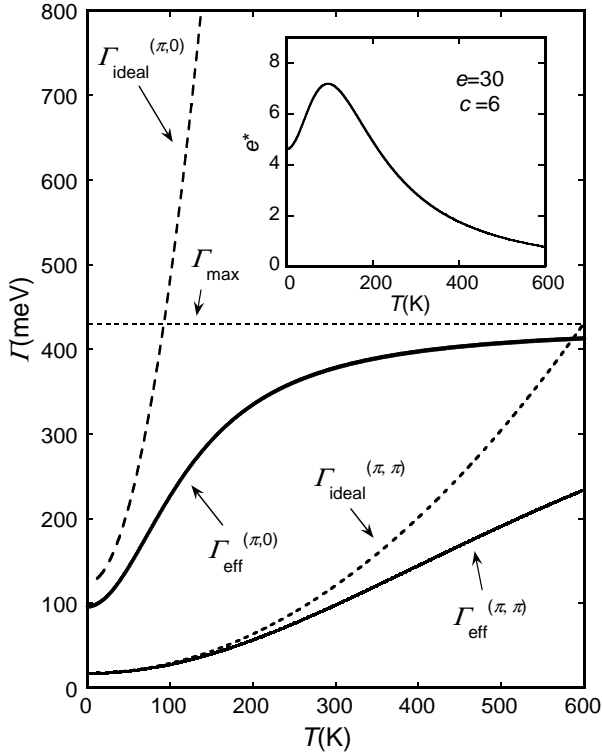


FIG. 1. T -dependence of the ideal and effective scattering rates for $(\pi, 0)$ and (π, π) within the model. The parameters used are given in the text. Inset: T -dependence of the effective anisotropy $e^* = \Gamma_{\text{eff}}^{(\pi,0)}/\Gamma_{\text{eff}}^{(\pi,\pi)} - 1$ for the same parameters

this way, the T -dependence of $e^*(T)$ mimics that of the Hall coefficient $R_H(T)$ in HTC.

III. FITTING

A. Application to Tl2201

Tl2201 is an ideal system for modelling the normal state transport properties in HTC for several important reasons; (i) Tl2201 is a single band cuprate, and therefore does not contain any secondary conducting subsystem, such as the CuO chains that complicate Hall and/or MR data in $\text{YBa}_2\text{Cu}_3\text{O}_{7-\delta}$ (YBCO); (ii) having a single CuO_2 plane, bilayer coupling is irrelevant; (iii) the doping range of Tl2201 covers only the OD region of the phase diagram thereby avoiding any further complications due to the normal state pseudogap; (iv) a T -dependent anisotropy in the in-plane scattering rate has already been observed in OD Tl2201 ($T_c = 30\text{K}$) from c -axis MR measurements;¹⁶ and finally (v) $\rho_{ab}(T)$ and $\cot\Theta_H(T)$ exhibit the very clean linear and quadratic T -dependencies characteristic of OP cuprates as shown in Fig. 2 (the experimental data are represented by closed circles).^{21,22} One surprising feature of the experimental data is the small *negative* zero-temperature intercept

in $\rho_{ab}(T)$ (extrapolation indicated by a dotted line) co-existing with a large *positive* intercept in $\cot\Theta_H(T)$. Line fits to the experimental data between 130K and 300K actually give $\rho_{ab}(T) = -10 + 1.56T$ ($\mu\Omega\text{cm}$) and $\cot\Theta_H(T) = 27 + 0.0014T^2$ (in 10 Tesla).²¹ This subtle but important feature has often been overlooked but as will be shown, is a natural consequence of the form of the scattering rate presented here.

To complete the Boltzmann transport analysis, I introduce a Fermi wave vector k_F and Fermi velocity v_F consistent with band structure calculations,²³ i.e. $k_F(\phi) = 6.5(1 + 0.15 \sin^2 2\phi) \text{ \AA}^{-1}$ and $v_F(\phi) = 2.5(1 + 0.2 \sin^2 2\phi) \times 10^5 \text{ ms}^{-1}$. This expression for $k_F(\phi)$ is consistent with a hole doping concentration $p = 0.16$. The small anisotropy factors do not play a significant role in the following analysis and for simplicity, both $k_F(\phi)$ and $v_F(\phi)$ are assumed to be independent of doping concentration. The corresponding saturation scattering rate $\Gamma_{\text{max}}(\phi) = 650(1 + 0.2 \sin^2 2\phi) \text{ THz}$ or $435(1 + 0.2 \sin^2 2\phi) \text{ meV}$ (since $a = 3.86 \text{ \AA}$). Note that the value of Γ_{max} is entirely determined by our choice of v_F and contains the same anisotropy factor as v_F to ensure that the condition $\ell = a$ is satisfied everywhere. Again, these values are kept constant for all doping concentrations investigated here. Thus in the ensuing analysis, there are only four adjustable parameters, namely the two anisotropy parameters c and e and the coefficients of $\Gamma_{\text{ideal}}(T)$, α and β . The choice of α and β is somewhat restricted however since according to the Ong representation, α and β should be comparable with the coefficients A and B determined from $\cot\Theta_H(T)$. These four parameters are then adjusted to obtain the best global fits, labelled hereafter $\rho_{ab}^{\text{fit}}(T)$, $\cot\Theta_H^{\text{fit}}(T)$ and $\Delta\rho_{ab}^{\text{fit}}/\rho_{ab}^{\text{fit}}(T)$, to the three independent transport properties $\rho_{ab}(T)$, $\cot\Theta_H(T)$ and $\Delta\rho_{ab}/\rho_{ab}(T)$. Finally, scaling corrections of the order 30% were allowed in the fits to account for any systematic errors in the experimentally determined quantities.

The solid lines in Fig. 2 are $\rho_{ab}^{\text{fit}}(T)$ and $\cot\Theta_H^{\text{fit}}(T)$ for OP Tl2201. The fitting parameters used are $\alpha = 27 \text{ THz}$, $\beta = 0.00175 \text{ THz/K}^2$, $c = 6$ and $e = 30$. Above 130K, both the linear resistivity and the quadratic Hall angle are reproduced with slopes and (extrapolated) $T = 0$ intercepts in excellent agreement with the experimental data. Below 130K, $\rho_{ab}^{\text{fit}}(T)$ deviates from linearity, approaching T^2 as $T \rightarrow 0$, whilst $\rho_{ab}(T)$ actually shows a downward deviation from linearity below 130K, presumably due to the onset of superconducting fluctuations which always dominate the intrinsic behavior of the normal state $\rho_{ab}(T)$ near T_c . Note that the T dependence of $\Gamma_{\text{ideal}}(T) (= 27 + 0.00175T^2)$ is similar to that of $\cot\Theta_H(T) (= 27 + 0.0014T^2)$, in good agreement with Ong's picture.¹⁷

The insets in Fig. 2 show $\rho_{ab}^{\text{fit}}(T)$ and $\cot\Theta_H^{\text{fit}}(T)$ over an extended temperature range up to 500K. The influence of Γ_{max} on the high- T behavior is manifest as a slight deviation from linearity above 360K, indicating the onset of saturation in $\Gamma_{\text{eff}}(T)$. The fact that this tendency

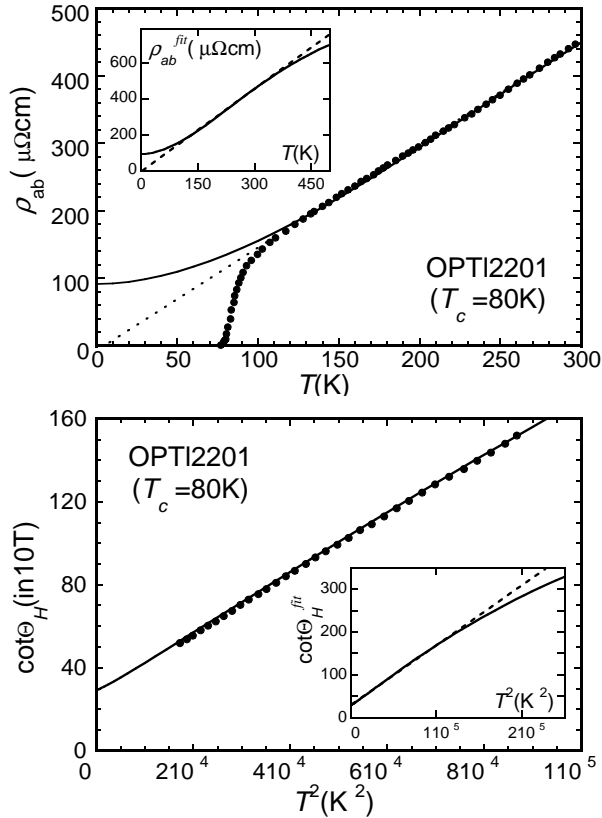


FIG. 2. Top: $\rho_{ab}(T)$ (closed circles) and $\rho_{ab}^{fit}(T)$ (solid line) for OP Tl2201.²¹ The dotted line is an extrapolation of $\rho_{ab}(T)$ to $T = 0\text{K}$. Bottom: $\cot\Theta_H(T)$ (closed circles) and $\cot\Theta_H^{fit}(T)$ for the same crystal.²¹ Insets: The same fits up to 500K, showing the onset of saturation at higher T .

towards saturation is not actually observed in $\rho_{ab}(T)$ indicates that the model does not capture all the essential physics. However, as I argue in section IV, there are several possible factors that might lead to a non-saturating resistivity in HTC which go beyond conventional Boltzmann transport analysis and may mask the intrinsic behavior of the scattering rate at higher temperatures.

The modified Kohler's rule $\Delta\rho_{ab}/\rho_{ab} = m^2 \tan^2\Theta_H$ is also obeyed in OP Tl2201, with $m \sim 1.9$ down to 130K,²² as shown by the dashed line in Fig. 3. (Below this temperature, superconducting fluctuations again begin to dominate.) This value lies in between the experimentally determined values for OP $\text{La}_{2-x}\text{Sr}_x\text{CuO}_4$ (LSCO)³ and OP YBCO³ indicated by dotted lines in Fig. 3. The open circles in the figure are $m^{fit}(T)$ for OP Tl2201 calculated using the same model parameters that were used in Fig. 2. As can be seen, $m^{fit}(T)$ has the correct magnitude and T -dependence, decreasing by only 10% between 0K and 300K. Note that the present model does not include vertex corrections nor paraconductivity contributions that might influence the form of $\Delta\rho_{ab}/\rho_{ab}(T)$ at low T .

The behavior of $m^{fit}(T)$ is determined almost exclu-

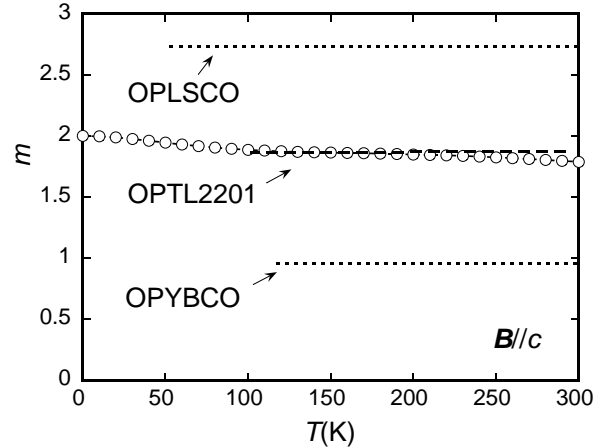


FIG. 3. Dashed line: Modified Kohler's plot $m(T)$ for OP Tl2201 (where $m^2 = (\Delta\rho_{ab}/\rho_{ab})/\tan^2\Theta_H$).²² The open circles represent $m^{fit}(T)$ obtained with the same fitting parameters as used in Fig. 2. Dotted lines: $m(T)$ for OP LSCO and YBCO.³

sively by the anisotropy parameters c and e . (If $c = 0$, for example, $\Delta\rho_{ab}^{fit}/\rho_{ab}^{fit}(T)$ would fall steeply as $T \rightarrow 0$.) The large value of e is surprising, but is necessary, not only to give the correct magnitude for m at finite temperatures, but also to maintain a robust T^2 dependence of $\cot\Theta_H^{fit}(T)$. Hence, within this model, the observation of a quadratic Hall angle and the form of $\Delta\rho_{ab}^{fit}/\rho_{ab}^{fit}(T)$ are all signatures of an extremely anisotropic basal plane scattering rate that likewise varies as T^2 . The T -linear resistivity, on the other hand, is simply an artefact of the broad crossover between the (approximately) T^2 resistivity at low T and the saturation of Γ_{eff} at high T .

The ability of the present model to reproduce the correct magnitude and T -dependence of the orbital MR is to be contrasted with the 'Cold Spots' model⁷ where the parameters required to separate the transport and Hall lifetimes yield an orbital MR that is orders of magnitude too large and has a much stronger T -dependence than shown in Fig. 3. This difficulty is overcome in the present model by the introduction of the shunt Γ_{max} that makes the effective anisotropy around the Fermi surface much smaller (see inset to Fig. 1), thereby reducing both the magnitude and the T -dependence of $\Delta\rho_{ab}^{fit}/\rho_{ab}^{fit}(T)$.

The evolution of the normal state transport properties in Tl2201 with doping are summarized in Fig. 4. The top panel in Fig. 4 shows $\rho_{ab}(T)$ (closed circles) and $\rho_{ab}^{fit}(T)$ (solid lines) for two OD Tl2201 single crystals with T_c values of 55K and 30K.²² The parameters used in these fits are $\alpha = 9$ THz, $\beta = 0.0016T^2$ THz/K², $c = 2$ and $e = 11.5$ for the 55K crystal, and $\alpha = 7$ THz, $\beta = 0.0015T^2$ THz/K², $c = 2$ and $e = 8$ for the 30K crystal. Note that the anisotropy factors are markedly reduced compared to OP Tl2201, reflecting the increased curvature observed in $\rho_{ab}(T)$. The bottom panel in Fig. 4 shows the corresponding $\cot\Theta_H(T)$ and $\cot\Theta_H^{fit}(T)$ for the two samples.

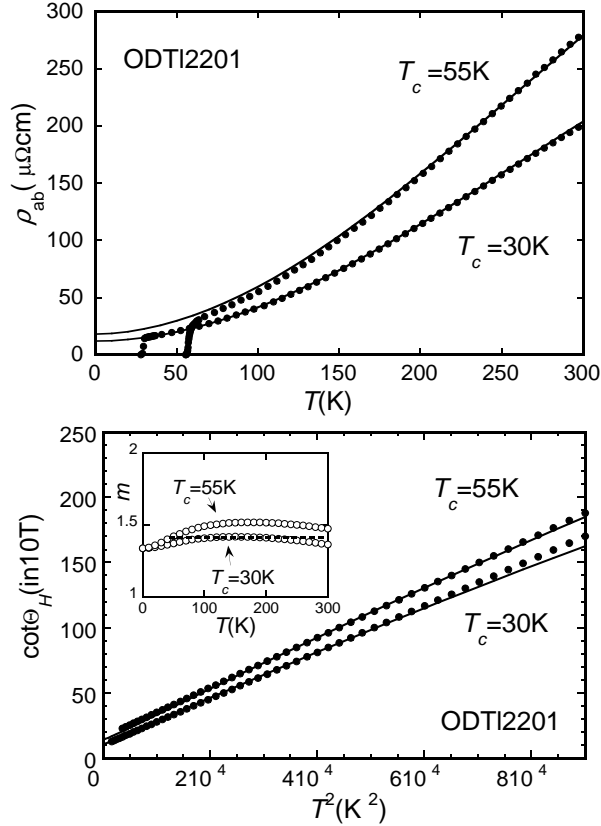


FIG. 4. Top: $\rho_{ab}(T)$ ²² (closed circles) and $\rho_{ab}^{fit}(T)$ (solid lines) for OD Tl2201 ($T_c = 55\text{K}$ and $T_c = 30\text{K}$). Bottom: $\cot\Theta_H(T)$ ²² (closed circles) and $\cot\Theta_H^{fit}(T)$ (solid lines) for the same samples with the same fitting parameters. Inset: $m^{fit}(T)$ (open circles) for the two sets of parameters. The dashed line represents the experimental data for the 30K crystal.²²

In contrast to OP Tl2201, $\cot\Theta_H^{fit}(T)$ deviates slightly from a simple T^2 dependence. In fact, the T -dependence is closer to $T^{1.95}$ and $T^{1.9}$ for the 55K and 30K crystals respectively. This deviation from a T^2 dependence reflects the fact that in less anisotropic cuprates, other regions of the Fermi surface are beginning to contribute to the Hall angle. The inset in the bottom panel of Fig. 4 gives the modified Kohler's plot derived for the two doping levels. As we expect, m^{fit} is lower in these examples compared with OP Tl2201, with values approaching 1.55 and 1.4 for the 55K and 30K crystal respectively. Experimentally, m is found to be 1.4 for 30K Tl2201 (indicated by a dashed line),²² again in excellent agreement with the model.

B. Application to Bi2212

With its improved energy and momentum resolution, ARPES has become a powerful probe of the single-particle self-energy Σ of HTC. The vast majority of work to date has been carried out on the bilayer cuprate

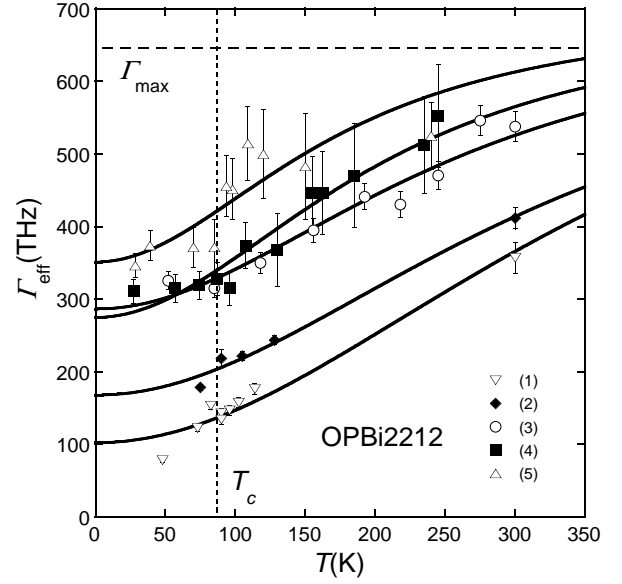


FIG. 5. Quasi-particle scattering rate for OP Bi2212 extracted from ARPES measurements.²⁶ The various numbers and symbols refer to different locations on the Fermi surface as described in the text. The solid lines are fits to the individual scattering rates using the expression for $\Gamma_{\text{eff}}(\phi, T)$.

Bi2212, due to its ease of cleaving. One of the most striking features of the emerging spectral function in Bi2212 is the broad featureless normal state spectrum at $(\pi, 0)$ whose lineshape sharpens dramatically into the well-known peak-dip-hump structure upon cooling below T_c . Although interpretation of ARPES spectra is still a controversial topic,²⁴ it has been argued^{7,25} that this dramatic rearrangement of the ARPES lineshape indicates the presence of ill-defined quasi-particle states in the normal state at $(\pi, 0)$, rendered incoherent by some form of catastrophic low-energy scattering mechanism. ARPES data also reveal that the broadening of the quasi-particle self-energy is much less dramatic for quasi-particles at (π, π) and that this basal plane anisotropy is much larger for OP cuprates than for OD cuprates.¹⁵ All these features indicate a highly anisotropic normal state scattering rate whose anisotropy grows weaker with overdoping, consistent with the picture described above for Tl2201.

Fig. 5 shows the variation of the quasi-particle scattering rate with angle and temperature for an OP Bi2212 single crystal, extracted from the ARPES data of Valla *et al.*²⁶ The various symbols shown in Fig. 5 are the same as those used in the original Valla plot of the momentum widths Δk , obtained in turn by fitting different momentum distribution curves (MDC) with Lorentzian line shapes. The quasi-particle scattering rates $1/\tau$ are obtained using the usual expression $1/\tau = 2\text{Im}\Sigma = \hbar\Delta k v_k$ where $\text{Im}\Sigma$ is the imaginary part of the single-particle self energy and v_k is the unrenormalized band velocity $\sim 4.0 \times 10^5 \text{ms}^{-1}$. The numbers refer to locations on the Fermi surface at angles, (1) = 45° , (2) = 37.5° , (3) = 25.5° , (4) = 17.5° and (5) = 7° away from $(\pi, 0)$.

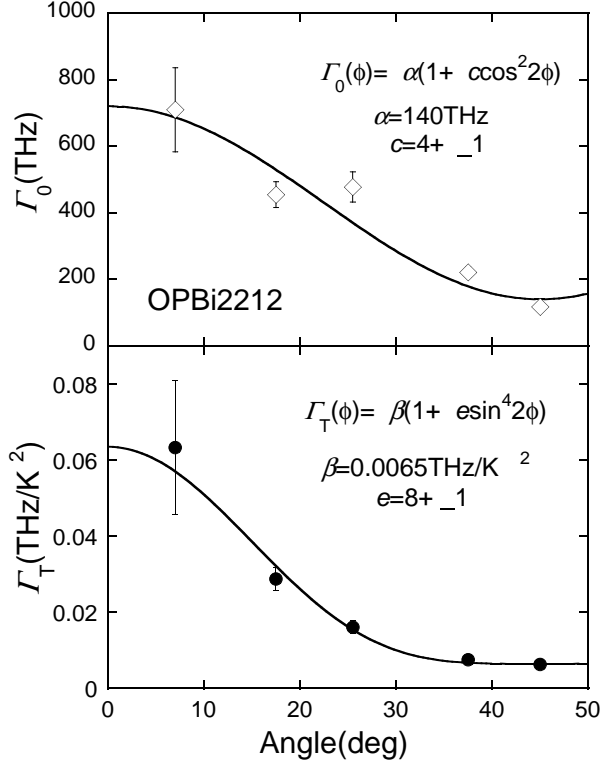


FIG. 6. Angular dependence of Γ_0 (top panel) and Γ_T (bottom panel) for OP Bi2212 determined from the fits to the MDC curves shown in Fig. 5. The solid lines are best fits whose expressions are shown in the appropriate figures.

The normal state Fermi velocity, determined at each location from the slope of the dispersion relation near the Fermi level, can be approximated by the expression $v_F(\phi) = 2.5(1 + 0.2 \sin^2 2\phi) \times 10^5 \text{ ms}^{-1}$.²⁶ Note that this is the same $v_F(\phi)$ used in the Tl2201 analysis. Similarly, $\Gamma_{\max}(\phi) = 650(1 + 0.2 \sin^2 2\phi) \text{ THz}$ or $435(1 + 0.2 \sin^2 2\phi) \text{ meV}$.

The solid lines in Fig. 5 are the fits to the ARPES data using the model scattering rate $\Gamma_{\text{eff}}(\phi, T)$. The fits are all reasonable and give angular dependencies for the resulting $\Gamma_0(\phi)$ and $\Gamma_T(\phi)$ as shown in Fig. 6. The solid lines in Fig. 6 are weighted fits to the expressions $\Gamma_0(\phi) = \alpha(1 + c \cos^2(2\phi))$ and $\Gamma_T(\phi) = \beta(1 + e \sin^4(2\phi))$ with $\alpha = 140 \text{ THz}$, $\beta = 0.0065 \text{ THz/K}^2$, $c = 4 \pm 1$ and $e = 8 \pm 1$. Note that $\Gamma_T(\phi)$ is more strongly peaked at $(\pi, 0)$ than $\Gamma_0(\phi)$. The reason these anisotropy factors seem large is the presence of Γ_{\max} . As $\Gamma_{\text{eff}}(\phi, T)$ approaches Γ_{\max} , $\Gamma_{\text{ideal}}(\phi, T)$ must change significantly in order to create even a small change in $\Gamma_{\text{eff}}(\phi, T)$. Hence within this model, the ‘ideal’ scattering rate is actually much more anisotropic than the raw data suggest.

The form of $\Gamma_{\text{eff}}(\phi, T)$ obtained above is inserted into the Boltzmann equation to obtain a crude estimate of $\rho_{ab}^{\text{fit}}(T)$ and $\cot\Theta_H^{\text{fit}}(T)$ as shown in the top panel of Fig. 7. The resistivity has a very large zero-temperature offset though is approximately linear from T_c up to $T = 250 \text{ K}$ at which point, $\rho_{ab}^{\text{fit}}(T)$ tends towards saturation as the

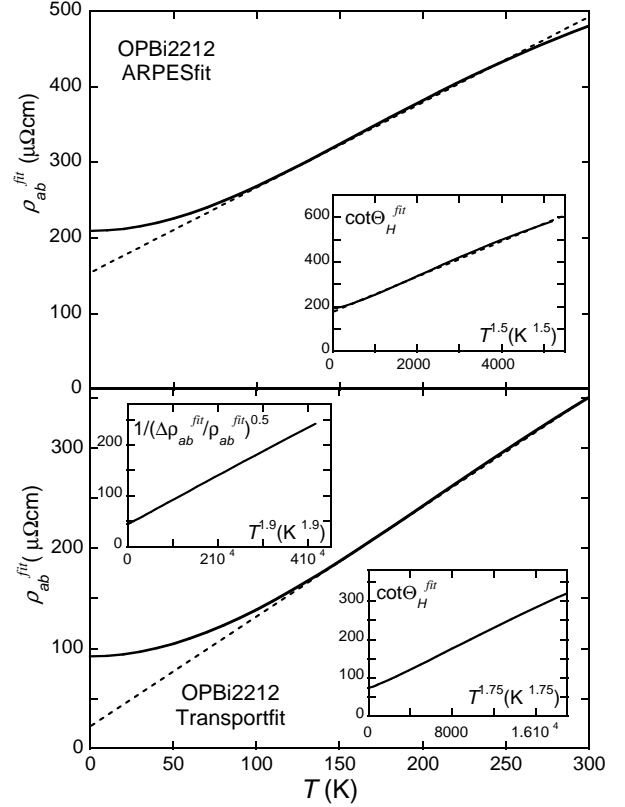


FIG. 7. Top panel: $\rho_{ab}(T)$ and $\cot\Theta_H(T)$ (inset) for OP Bi2212 using the fitting parameters derived from the ARPES data. *Solid circles*: the results from the model, *dashed lines*: guides to the eye. Bottom panel: Best fits to $\rho_{ab}(T)$ (main figure) $\cot\Theta_H(T)$ (top inset) and $1/(\Delta\rho_{ab}/\rho_{ab})^{0.5}(T)$ (bottom inset) for OP Bi2212. Note the different T -dependencies of the various plots.

effect of Γ_{\max} becomes prominent. $\cot\Theta_H^{\text{fit}}(T)$, on the other hand, is found to vary roughly as $A + BT^{1.5}$. Experimentally, $\rho_{ab}(T)$ in OP Bi2212 shows the ubiquitous T -linear behavior, but has a *positive* zero-temperature intercept, indicative of increased inhomogeneity in this compound,²⁷ whilst $\cot\Theta_H(T) = A + BT^n$ where $n = 1.75 \pm 0.05$,^{28,14} in contrast to the usual result for OP cuprates, $n = 2$. Similar behavior is also observed in Bi2201.^{13,14}

Whilst the ARPES-derived fits are in reasonable agreement with the experimental data, they are not ideal. In any case, one does not expect the transport scattering rate to be equivalent to the single-particle scattering rate obtained by ARPES, since the former should be dominated by large-angle scattering events whilst the latter will not. The best actual fits to the transport data for OP Bi2212²⁹ are shown in the bottom panel of Fig. 7 for the fitting parameters $\alpha = 50 \text{ THz}$, $\beta = 0.00325 \text{ THz/K}^2$, $c = 4$ and $e = 8$. These values give the expected linear resistivity between T_c and 300K with the correct slope and intercept and $\cot\Theta_H^{\text{fit}}(T) = A + BT^{1.75}$ over the entire temperature range, again with the correct slope

and intercept. The deviation of $\cot\Theta_H(T)$ from its simple T^2 dependence arises from the increased disorder in Bi2212 that must somehow smear out the anisotropy of the scattering rate around the Fermi surface. Note that the anisotropy factors are exactly the same as those obtained from the ARPES data, while β in the transport fit is half the ARPES value. The much larger residual scattering rate inferred from the ARPES spectra is a common feature of photoemission data¹¹ so is not unexpected. Incidentally, using the same parameters, $\Delta\rho_{ab}^{fit}/\rho_{ab}^{fit}(T)$ is found to vary as $(C + DT^{1.9})^{-2}$, also shown in Fig. 7. This is only a prediction from the model at present since $\Delta\rho_{ab}/\rho_{ab}(T)$ has yet to be established experimentally in OP Bi2212.

It should be stressed finally that the ARPES measurements of Valla *et al.*²⁶ are often cited as strong evidence for a *linear* quasi-particle scattering rate in HTC that is itself responsible for the T -linear resistivity observed at optimal doping. However, as noted by Valla and co-workers, near the anti-nodal point (label number (5) in Fig. 5), the scattering rate becomes almost T -independent. This tendency towards saturation is an essential part of the present model, and combined with a single scattering rate that is *quadratic* in temperature everywhere on the Fermi surface, it is able to account for the quasi-linear scattering rate at the nodes (Fig. 5), the T -linear resistivity, the tendency towards saturation at $(\pi, 0)$ and an inverse Hall angle that varies as $A + BT^{1.75}$, without requiring any additional assumptions. Note that in the Cold-Spots model, the scattering rate at the nodes is always quadratic, whilst in the MFL phenomenology, there is no saturation at $(\pi, 0)$.

IV. DISCUSSION

It is clear that the physical mechanism behind the normal state scattering rate, and *ipso facto* high-temperature superconductivity, can only be determined once a coherent description of all the normal state transport properties in HTC is found. In this paper, I have outlined a new phenomenology that shows promising signs of achieving this goal. However, whilst many of the anomalous features can be explained within this simple model, the current proposal appears, at first sight at least, to be incompatible with two key aspects of the experimental situation in HTC; namely the linear resistivity at low T and the absence of resistivity saturation at high T . Therefore, before going on to discuss the possible implications of the model, it is perhaps worth outlining to the reader how these two major discrepancies might possibly be reconciled.

It has often been claimed that $\rho_{ab}(T)$ in OP cuprates is linear at all finite temperatures. This long-held view is based largely on the observation back in 1990 of a linear $\rho_{ab}(T)$ in single crystal Bi2201 extending from 700K down to $T_c = 10\text{K}$.³⁰ If this were indeed the intrinsic be-

havior, it would certainly require an explanation outside the realms of conventional FL physics. Important new data on the latest generation of Bi2201 crystals (with significantly improved T_c values) tell a rather different story however. By suppressing superconductivity in OP Bi2201 ($T_c = 32\text{K}$) in a 60 Tesla pulsed magnetic field, Ono *et al.*³¹ recently found that the linear $\rho_{ab}(T)$ seen at high T (and giving an apparent zero intercept at $T = 0\text{K}$) crosses over to a higher power T -dependence below around 60K, before saturating at some finite *positive* ρ_0 . Similar behavior has also been reported in OP LSCO.³² The extension of the linear $\rho_{ab}(T)$ to low temperatures in Bi2201 and LSCO (in zero-field) is not therefore intrinsic and is presumably caused by the onset of fluctuation conductivity, as is evident in the $\rho_{ab}(T)$ data of Tl2201 and Bi2212. In addition, the (extrapolated) negative intercept in $\rho_{ab}(T)$ found in the best quality Tl2201 and YBCO crystals^{21,33} is unphysical and dictates that $\rho_{ab}(T)$ *must* cross over to a higher power of T at lower temperatures. Such behavior is incompatible with the MFL hypothesis, for example, but is a natural consequence of the form of $\Gamma_{\text{eff}}(\phi, T)$ presented here. Perhaps in the light of these new results, the long-standing assertion that $\rho_{ab}(T)$ obeys a simple linear T -dependence at low T should now be re-examined. It would certainly be interesting to follow the T -dependence of OP cuprates with higher T_c to lower temperatures, as and when larger magnetic fields become available.

I now turn to address the second point, namely the absence of resistivity saturation at higher temperatures. The MIR limit and the parallel-resistor model have been applied successfully to a wide range of materials over the years. Their relevance to strongly correlated electron systems such as HTC, however, has been challenged in recent times.³⁴ In these so-called ‘bad metals’, $\rho(T)$ does not saturate. Instead $\rho(T)$ grows approximately linearly with T at high temperatures (typically $T > 300\text{K}$) reaching values of the order 1 - 10 m Ωcm that correspond to $\ell \ll a$. It is claimed that this absence of resistivity saturation is a signature of a non-FL ground state at zero temperature.³⁴ At first sight, these arguments appear rather compelling. However, the origin of the non-saturating resistivity in these systems is still poorly understood. More importantly, similar $\rho(T)$ behavior has also been reported in Sr_2RuO_4 ,³⁵ a close structural analog of the cuprates which exhibits quantum oscillations³⁶ and so forms a well-defined FL ground state at low T . The association of non-saturating $\rho(T)$ with a non-FL ground state is therefore misleading and that some other physical origin must be sought for the high- T behavior.

Possible sources for the excess resistivity include thermal expansion effects (known to play a significant role in the organic conductors, for example), a thermally-induced reduction in the density of states or carrier concentration, and the onset of a ‘thermal’ diffusive (non-Boltzmann) transport regime at high T that sets in once the concept of a scattering rate is no longer applicable and temperature becomes the only relevant energy

scale in the problem. Determining the origin of this non-saturating resistivity, though desirable, is not essential for justifying the model however, since the current model is only strictly applicable in the low- T ($T < 300\text{K}$) regime, where the majority of the carriers are still well-defined quasi-particles and Boltzmann transport analysis remains valid.

Any observation of a threshold in the scattering rate would obviously lend significant weight to the arguments presented here however. In addition to the work of Valla *et al.*,²⁶ Norman *et al.* have recently extracted $\text{Im}\Sigma$ along $(\pi, 0)$ for slightly OD Bi2212²⁵ and found that it too saturates above T_c at a value $2\text{Im}\Sigma_{\text{max}} \sim 180$ meV, well within the range of validity given by $\ell = a$. Optical measurements can also be used in principle to separate Γ from the conductivity, though here the situation is not as clear. In particular, Γ is found to saturate with increasing temperature, but NOT with increasing frequency.³⁷ Finally, recent analysis of the plasmon spectra in K_3C_{60} ,³⁸ another system with non-saturating resistivity, has revealed that the quasi-particle scattering rate itself saturates around $T = 500\text{K}$ at a value $\Gamma_{\text{max}} \sim 450$ meV. Whilst more experimental work is clearly required to clarify this effect, these observations do point to the possibility that the MIR limit may still be a preserve of *all* metallic systems, in the strictest sense that Γ never exceeds the maximum value Γ_{max} corresponding to $\ell = a$, and that the excess resistivity seen in these strongly correlated systems should not be regarded simply as a signature of an ever-increasing scattering rate. Moreover, since the phenomenology described in this paper has been shown to provide a coherent description of many of the anomalous normal state transport properties in HTC, further efforts to separate $\Gamma(T)$ from $\rho(T)$ are strongly recommended.

Turning now to the implications of the model, the most striking features of the analysis on Tl2201 are clearly the large values for c and e and their strong variation with doping, as summarized in Fig. 8. (For each crystal, the doping level p is obtained from the well-known HTC parabola law $T_c(p)/T_c^{\text{max}} = 1 - 82(p - 0.16)^2$,³⁹ shown as a solid line in Fig. 8.)

The large value of c , particularly at optimum doping, is somewhat surprising, though it is not inconsistent with the picture emerging from ARPES measurements on Bi2212.²⁶ Recently it has been argued¹⁰ that scattering on impurities located *off* the CuO_2 planes may be the source of this four-fold anisotropy in $\Gamma_0(\phi)$. In the case of tetragonal Tl2201, such interplane randomness might be induced by Tl/Cu site substitutions as well as by interstitial oxygen. It is not clear at this stage why such large anisotropy would also appear in the transport scattering rate, which typically depends only on large-momentum transfers. However, as noted by Varma and Abrahams,¹⁰ such anisotropic elastic scattering may well play a key role in the *magneto*-transport behavior. Indeed, the large value of c is only required in the fitting here to maintain the constancy of $m^{fit}(T)$ down to low

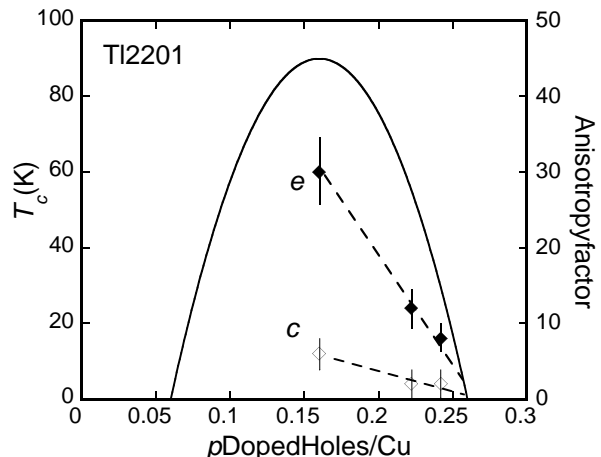


FIG. 8. Variation of the anisotropy factors c (open diamonds) and e (closed diamonds) with doping concentration p . The dashed lines are guides to the eye. The solid line represents the $T_c(p)$ parabola for HTC.³⁹ The error bars reflect the range of fitting parameters that provide a reasonable fit to all three transport coefficients.

temperatures.

The T -dependent anisotropy factor e is found to drop steeply from optimal doping, scaling approximately with T_c and approaching zero close to the doping level where superconductivity vanishes. This is to be expected perhaps, since the separation of transport and Hall lifetimes is observed to vanish in the most highly OD samples.⁴⁰ The correlation between $e(p)$ and $T_c(p)$ on the OD side is intriguing and suggests that the mechanism giving rise to this strongly anisotropic scattering rate might also be associated with the anisotropy (d -wave pairing symmetry) of the superconducting order parameter.

As illustrated in Fig. 1, $\Gamma_{\text{ideal}}^{(\pi,0)}(T)$ for OP Tl2201 is found to cross the MIR limit close to $T = T_c$. ($\Gamma_{\text{eff}}^{(\pi,0)}(T)$ will obviously be lower than the MIR limit due to the presence of the shunt Γ_{max} .) The same is also true for OP Bi2212. The picture that emerges therefore is one in which the quasi-particles at $(\pi, 0)$ are approaching an incoherent state at $T = T_c$, consistent with what is observed in ARPES, and this may well have implications for the onset temperature of superconductivity on the underdoped (UD) side of the phase diagram. More explicitly, if e continues to grow with decreasing p , the temperature at which the anti-nodal quasi-particles become incoherent will decrease accordingly. What ultimately causes the suppression of T_c on the UD side of the phase diagram is still an open issue, and I cannot address that important question here, since clearly, the physics of the UD cuprates is also heavily influenced by the opening of the pseudogap which cannot yet be accounted for within this simple phenomenological model. Nevertheless, the onset of incoherent quasi-particles at $T = T_c^{\text{max}}$ is an intriguing observation from the above analysis, hints at a new interpretation of the $T_c(p)$ parabola across the HTC phase diagram and should be investigated further.

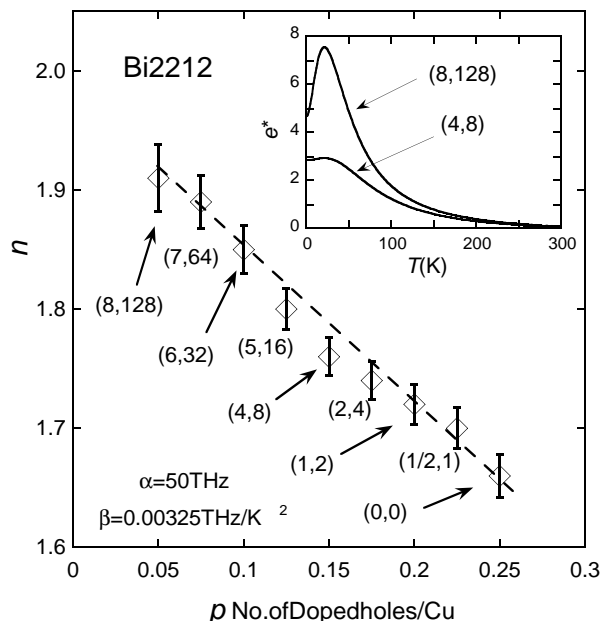


FIG. 9. Simulation of the variation of $n(p)$ for Bi2212 where n is the coefficient of inverse Hall angle $\cot\Theta_H(T) = A + BT^n$. The anisotropy factors (c, e) used in the fitting routines are indicated in parentheses. The dashed line is a guide to the eye.¹⁴ Inset: Effective anisotropy $e^*(T)$ for two selected points.

Some possible insight into the nature of the scattering on the UD side can be gained from further analysis of the Hall angle in Bi2212. In recent detailed transport studies of the Bi-based cuprates Bi2212 and Bi2201, $\cot\Theta_H(T)$ was found to vary as T^n with n decreasing from $n \sim 2$ to $n \sim 1.6 - 1.7$ as one moves from the UD to the OD regime. This non-universal power law behavior in $\cot\Theta_H(T)$ reveals a new layer of complexity in the phenomenology of normal state transport in HTC that has yet to be addressed. It was noted earlier for Tl2201, that n decreases on the OD side as c and e are reduced. Given that at optimal doping, $n \sim 1.8$ lies roughly in the middle of the variable range for Bi2212, it is tempting to attribute this variation in $n(p)$ purely to changes in c and e across the phase diagram. A simple example of how this might come about is illustrated in Fig. 9 where c and e have been varied systematically to simulate the experimentally observed variation of n with doping,¹⁴ whilst keeping α and β fixed at the values extracted from the transport fits for OP Bi2212 in Fig. 7. Intriguingly, in the isotropic case $c = e = 0$, $n \sim 1.65$, in agreement with the experimental data. As c and e are increased, n rises as expected, but only approaches $n = 2$ for extremely large values of e . Whilst this example is not completely rigorous, it does suggest that with more careful analysis, the systematic variation of n with doping in Bi2212 and Bi2201, and its range of values, might be understood within this simple model. It also implies that the anisotropy of the T^2 scattering

rate must increase (almost exponentially) with decreasing doping on the UD side, reaching values greater than 100 for $p \sim 0.05$! Indeed, within the present model, it is the *only* way to account for the observation of $\cot\Theta_H(T) = A + BT^2$ in UD Bi2212. However, as illustrated in the inset of Fig. 9, the effective anisotropy $e^*(T)$ above 100K is almost indistinguishable for the OP and the most UD cases. Hence, whilst e may increase dramatically, the more experimentally accessible quantity e^* does not.

Comparison of the fitting parameters for OP Bi2212 and OP Tl2201 reveal another important aspect of the modelling. The degree of anisotropy in OP Bi2212 ($c = 4$, $e = 8$) is markedly reduced compared with that in OP Tl2201 ($c = 6$, $e = 30$) whilst the coefficients of $\Gamma_{\text{ideal}}(T)$ ($\alpha = 50$ (27) and $\beta = 0.00325$ (0.00175) for OP Bi2212 (OP Tl2201)) are increased. This implies that the strength of the scattering rate, averaged around the Fermi surface, is very similar in the two cases, but the higher degree of disorder and inhomogeneity in Bi2212, evidenced by the larger value of α (the level of impurity scattering at the nodal points) acts to smear out this strong anisotropy.

Whilst I do not wish to speculate at this stage on the origin of $\Gamma_{\text{eff}}(\phi, T)$, there are still some important remarks that can be made from the above analysis. Firstly, the strong anisotropy and T^2 dependence of $\Gamma_{\text{eff}}(\phi, T)$ strongly suggests that the dominant scattering rate in HTC is electronic in origin and that electron-phonon scattering plays only a minor role in the normal state transport properties of HTC. The large increase in the quasi-particle lifetime below T_c observed in conductivity measurements^{41,42} is consistent with the disappearance of this catastrophic electronic scattering mechanism below T_c . Secondly, the large value for e for OP Tl2201 (Fig. 8) implies the existence of a singular scattering mechanism, peaked at $(\pi, 0)$, whose intensity grows rapidly with decreasing carrier concentration. Moreover, the striking growth of the intensity of the scattering at $(\pi, 0)$ as we move towards the antiferromagnetic (AFM) insulating state (Fig. 9) points to a scattering mechanism that is magnetic in origin, possibly due to some form of AFM spin fluctuations. Another potential candidate though, particularly given the form of the anisotropy and its singular nature, is the collective resonance mode seen in neutron scattering measurements on several cuprates, including Tl2201. Intriguingly, whilst the resonance mode is resolution limited, i.e. strongly peaked at $(\pi, 0)$ in Tl2201,⁴³ it is significantly broadened in k -space in Bi2212,⁴⁴ consistent with the conclusions derived above. It is noted with caution however, that this mode has so far only been unambiguously resolved below T_c , so its relevance to scattering in the normal state has yet to be established.

V. CONCLUSIONS

In summary, I have demonstrated how the seemingly anomalous dc transport properties of HTC may be accounted for consistently within a Boltzmann transport analysis with a single T^2 scattering rate that varies markedly around the basal plane. In particular, the separation of transport and Hall lifetimes, the modified Kohler's rule and the evolution of the transport properties across the OD region of the phase diagram can all be reproduced with a single set of parameters. In addition, the different T -dependence of the Hall angle observed in the Bi-based cuprates is shown to be simply an artefact of the increased inhomogeneity of these materials; the T^2 scattering rate continues to be the dominant source of scattering in Bi2212 but its singular nature is smeared out by the disorder. The form of $\Gamma_{\text{eff}}(\phi, T)$ is also consistent with several features of the single-particle spectral function identified by ARPES, including the strong basal plane anisotropy (both in the zero-temperature and the T -dependent scattering terms) and the tendency towards saturation along $(\pi, 0)$. Such a wide-ranging consistency with experiment is indeed encouraging and strongly suggests that a conventional Boltzmann transport approach might be more appropriate to describe the normal state of HTC (at least in the intermediate and low T ranges) than was previously imagined.

The fact that the parent HTC compound at half-filling is an AFM Mott insulator rather than a metal has pointed clearly to the role of strong electron correlations in the square planar CuO_2 lattice as a key element in the cuprate problem. The introduction of holes into a highly correlated 2D magnetic background is believed to give rise to a non-FL ground state at low doping, characterized by the highly anomalous physics of the UD cuprates, and ultimately, unconventional high temperature superconductivity. It has often been assumed moreover, that with continued doping, HTC eventually evolve into a conventional FL as the electron correlations become weaker and the system becomes more three-dimensional. In this paper, I have identified a form for the normal state scattering rate that although somewhat unconventional, is still rooted in FL physics, yet can explain the evolution of the normal state transport properties of OD HTC right up to optimum doping. Of course, I do not expect this simple model to remain valid on the UD side of the phase diagram, but if it shown to be applicable to the OD and OP cuprates, then the way in which this relatively simple picture breaks down, as the pseudogap opens and electron correlations become even stronger, might yet reveal the crucial missing link between the FL fixed point at large doping and the curious physics of HTC on the underdoped side.

VI. ACKNOWLEDGEMENTS

The author would like to acknowledge enlightening discussions with J.F. Annett, K. Behnia, A. Carrington, J.R. Cooper, I.R. Fisher, B.L. Gyorffy, J.W. Loram, A.P. Mackenzie, N. Nagaosa, K.G. Sandemann, A.J. Schofield, H. Takagi, J.L. Tallon and J.A. Wilson. The author also would like to acknowledge the hospitality of the University of Tokyo where many of these ideas were first formulated.

VII. APPENDIX: TRANSPORT COEFFICIENTS FOR A QUASI-2D FERMI SURFACE

The current response \mathbf{J}_i to an applied electric \mathbf{E} is given by

$$\mathbf{J}_i = \frac{1}{4\pi^3} \int e v_i g_k d^3k = \sigma_{ij} \mathbf{E}_j$$

where g_k is the displacement from the equilibrium distribution ($g_k = f - f_0$) due to the applied fields, σ_{ij} is the conductivity tensor and v_i is the Fermi velocity in the i direction. The total displacement can be summarized in the Bloch-Boltzmann transport equation, which under the relaxation time approximation, is given by

$$e\mathbf{E} \cdot \mathbf{v}_k \frac{\partial f_0}{\partial \varepsilon} + \frac{e}{\hbar} [\mathbf{v}_k \times \mathbf{B}] \frac{\partial g_k}{\partial k} = -g_k \Gamma$$

The various components of $\sigma_{ij}^{(n)}$ can be obtained through the Jones-Zener expansion

$$g_k^{(n)} = \left(-\frac{e}{\hbar\Gamma} [\mathbf{v}_k \times \mathbf{B}] \frac{\partial}{\partial k} \right)^n \left(\frac{e\mathbf{E} \cdot \mathbf{v}_k}{\Gamma} \left(-\frac{\partial f_0}{\partial \varepsilon} \right) \right)$$

to arrive at:

$$\sigma_{ij}^{(n)} = \frac{1}{4\pi^3} \int e v_i \left(-\frac{e}{\hbar\Gamma} [\mathbf{v}_k \times \mathbf{B}] \frac{\partial}{\partial k} \right)^n \frac{e v_j}{\Gamma} \left(-\frac{\partial f_0}{\partial \varepsilon} \right) d^3k$$

To calculate, for instance, the in-plane Hall conductivity $\sigma_{xy}^{(1)}$, we simply apply B_z and E_y and calculate the response J_x using the Jones-Zener term $g_k^{(1)}$.

For a quasi-2D Fermi surface, there are various techniques one can adopt to simplify the calculation. Firstly, the element d^3k is the product of an area parallel to the Fermi surface dS and a radial (in-plane) component dk_r , which is related to an incremental energy $d\varepsilon$ by

$$d\varepsilon = \hbar v_F \cdot k_F = \hbar v_F \cos \gamma dk_r$$

Here γ is the angle between v_F and dk_r (within the plane). Since v_F is always perpendicular to the Fermi surface, simple geometrical considerations give

$$\gamma(\phi) = \tan^{-1} \left[\frac{\partial}{\partial \phi} (\log k_F(\phi)) \right]$$

which is zero for a circular Fermi surface.

The element dS can be expanded into the cylindrical elements $k_F d\phi$ and dk_z to give

$$\int (-\frac{\partial f_0}{\partial \varepsilon}) d^3k = \int_0^{2\pi} \int_{-\pi/d}^{\pi/d} \frac{k_F}{\hbar v_F \cos \gamma}$$

for a quasi-2D Fermi liquid since $(-\partial f_0/\partial \varepsilon)$ is a delta function (provided all scattering is quasi-elastic). It is this integral $\int d\phi$ that will contain all the in-plane anisotropy of the essential parameters in our calculation. With $B \parallel c$, the cross-product $[\mathbf{v}_k \times \mathbf{B}] \partial/\partial k$ becomes $Bv_F \partial/\partial k_{\parallel}$ where

$$\frac{\partial}{\partial k_{\parallel}} = \frac{\cos \gamma}{k_F} \frac{\partial}{\partial \phi}$$

whilst for $B \parallel ab$, making an angle φ with the a -axis

$$[\mathbf{v}_k \times \mathbf{B}] \frac{\partial}{\partial k} = v_z [\hat{z} \times \mathbf{B}] \frac{\partial}{\partial k_{xy}} + [\mathbf{v}_{xy} \times \mathbf{B}] \frac{\partial}{\partial k_z}$$

i.e.

$$[\mathbf{v}_k \times \mathbf{B}] \frac{\partial}{\partial k} \approx Bv_F \sin(\phi - \gamma - \varphi) \frac{\partial}{\partial k_z}$$

Finally, it is noted that the tetragonal symmetry of Tl2201 allows the limits of integration to be reduced to 0 and $\pi/2$ by including an extra factor of 4.

Employing these simple techniques, one can now derive the individual terms of the in-plane and c -axis conductivity tensors. In this paper however, only the in-plane magneto-transport properties are considered and their formulae are listed below in the isotropic case. For the anisotropic case, simply replace v_F , k_F and Γ by $v_F(\phi)$, $k_F(\phi)$ and $\Gamma(\phi)$, or more appropriately for the present model, by $\Gamma_{\text{eff}}(\phi, T)$.

$$\sigma_{xx}^{(0)} = \frac{e^2}{4\pi^3 \hbar} \left(\frac{2\pi}{d}\right) 4 \int_0^{\pi/2} \frac{k_F v_F \cos^2(\phi - \gamma)}{\Gamma \cos \gamma} d\phi$$

$$\sigma_{xy}^{(1)} = \frac{-e^3 B}{4\pi^3 \hbar^2} \left(\frac{2\pi}{d}\right) 4 \int_0^{\pi/2} \frac{v_F}{\Gamma} \cos(\phi - \gamma) \frac{\partial}{\partial \phi} \left(\frac{v_F}{\Gamma} \sin(\phi - \gamma)\right) d\phi$$

$$\sigma_{xx}^{(2)} = \frac{e^4 B^2}{4\pi^3 \hbar^3} \left(\frac{2\pi}{d}\right) 4 \int_0^{\pi/2} \frac{v_F}{\Gamma} \cos(\phi - \gamma)$$

$$\frac{\partial}{\partial \phi} \left\{ \frac{v_F \cos \gamma}{\Gamma k_F} \frac{\partial}{\partial \phi} \left(\frac{v_F}{\Gamma} \cos(\phi - \gamma)\right) \right\} d\phi$$

The measurable quantities ρ_{ab} , $\tan \Theta_H$ and $\Delta \rho_{ab}/\rho_{ab}$ are obtained by inversion of the conductivity tensor:

$$\rho_{ab} = \frac{1}{\sigma_{xx}^{(0)}}$$

$$\tan \Theta_H = \frac{\rho_{xy}}{R_H B} \approx \frac{\sigma_{xy}^{(1)}}{\sigma_{xx}^{(0)}}$$

$$\frac{\Delta \rho_{ab}}{\rho_{ab}} = -\frac{\sigma_{xx}^{(2)}}{\sigma_{xx}^{(0)}} - \left(\frac{\sigma_{xy}^{(1)}}{\sigma_{xx}^{(0)}}\right)^2$$

-
- ¹ M. Gurvitch and A.T. Fiory, Phys. Rev. Lett. **59**, 1337 (1987).
 - ² T.R. Chien, Z.Z. Wang and N.P. Ong, Phys. Rev. Lett. **67**, 2088 (1991).
 - ³ J.M. Harris, Y.F. Yan, P. Matl, N.P. Ong, P. W. Anderson, T. Kimura and K. Kitazawa, Phys. Rev. Lett. **75**, 1391 (1995).
 - ⁴ A. Carrington, A.P. Mackenzie, C.T. Lin, and J.R. Cooper, Phys. Rev. Lett. **69**, 2855 (1992).
 - ⁵ B.P. Stojkovic and D. Pines, Phys. Rev. Lett. **76**, 811 (1996).
 - ⁶ C. Castellani, C. di Castro and M. Grilli, Phys. Rev. Lett. **75**, 4650 (1995).
 - ⁷ L.B. Ioffe and A.J. Millis, Phys. Rev. B **58**, 11631 (1998).
 - ⁸ P.W. Anderson, Phys. Rev. Lett. **67**, 2092 (1991).
 - ⁹ C.M. Varma, P.B. Littlewood, S. Schmitt-Rink, E. Abrahams and A.E. Ruckenstein, Phys. Rev. Lett. **63**, 1996 (1989).
 - ¹⁰ C.M. Varma and E. Abrahams, Phys. Rev. Lett. **86**, 4652 (2001).
 - ¹¹ T. Valla, A.V. Fedorov, P.D. Johnson, B.O. Wells, S.L. Hulbert, Q. Li, G.D. Gu, and N. Koshizuka, Science **285**, 2110 (1999).
 - ¹² A. Lanzara, P.V. Bogdanov, X.J. Zhou, S.A. Kellar, D.L. Feng, E.D. Lu, T. Yoshida, H. Eisaki, A. Fujimori, K. Kishio, J.-I. Shimoyama, T. Noda, S. Uchida, Z. Hussain and Z.-X. Shen, Nature **412**, 510 (2001).
 - ¹³ Y. Ando and T. Murayama, Phys. Rev. B **60**, R6991 (1999).
 - ¹⁴ Z. Konstantinovic, Z. Z. Li and H. Raffy, Phys. Rev. B **62**, R11989 (2000).
 - ¹⁵ Z.M. Yusuf, B.O. Wells, T. Valla, A.V. Fedorov, P.D. Johnson, Q. Li, C. Kendziora, Sha Jian and D.G. Hinks, Phys. Rev. Lett. **88**, 167006 (2002).
 - ¹⁶ N.E. Hussey, J.R. Cooper, J.M. Wheatley, I.R. Fisher, A. Carrington, A.P. Mackenzie, C.T. Lin, and O. Milat, Phys. Rev. Lett. **76**, 122 (1996).
 - ¹⁷ N.P. Ong, Phys. Rev. B **43**, 193 (1991).
 - ¹⁸ Z. Fisk and G.W. Webb, Phys. Rev. Lett. **36**, 1084 (1976).
 - ¹⁹ H. Wiesmann, M. Gurvitch, H. Lutz, A. Ghosh, B. Schwarz, M. Strongin, P.B. Allen and J.W. Halley, Phys. Rev. Lett. **38**, 782 (1977).
 - ²⁰ M. Gurvitch, Phys. Rev. B **24**, 7404 (1981).
 - ²¹ A.W. Tyler and A.P. Mackenzie, Physica **282-287C**, 1185 (1997).
 - ²² A.W. Tyler, PhD. thesis (University of Cambridge) (1997).
 - ²³ D.J. Singh and W.E. Pickett, Physica **203C**, 193 (1992).

- ²⁴ See, e.g., S.V. Borisenko, A.A. Kordyuk, S. Legner, C. Drr, M. Knupfer, M.S. Golden, J. Fink, K. Nenkov, D. Eckert, G. Yang, S. Abell, H. Berger, L. Forr, B. Liang, A. Maljuk, C.T. Lin, and B. Keimer, *Phys. Rev. B* **64**, 0904513 (2001).
- ²⁵ M.R. Norman, M. Randeria, H. Ding and J.C. Campuzano, *Phys. Rev. B* **57**, 11093 (1998).
- ²⁶ T. Valla, A.V. Fedorov, P.D. Johnson, Q. Li, G.D. Gu and N. Koshizuka, *Phys. Rev. Lett.* **85**, 828 (2000).
- ²⁷ T. Watanabe, T. Fujii and A. Matsuda, *Phys. Rev. Lett.* **79**, 2113 (1997).
- ²⁸ B. Beschoten, U. Rüdiger, J. Auge, C. Quitmann, H. Frank, H. Kurz and G. Güntherodt, *Physica C* **235-240**, 1373 (1994).
- ²⁹ The $\rho_{ab}(T)$ data used were the $\delta = 0.255$ data in Fig. 2 of ref.²⁷. The $\cot\Theta_H(T)$ data were the $p = 0.16$ sample shown in Fig. 3 of ref.¹⁴.
- ³⁰ S. Martin, A.T. Fiory, R.M. Fleming, L.F. Schneemeyer, and J.V. Waszczak, *Phys. Rev. B* **41**, 846 (1990).
- ³¹ S. Ono, Y. Ando, T. Murayama, F.F. Balakirev, J.B. Betts and G. S. Boebinger, *Phys. Rev. Lett.* **85**, 638 (2000).
- ³² G.S. Boebinger, Y. Ando, A. Passner, T. Kimura, M. Okuya, J. Shimoyama, K. Kishio, K. Tamasaku, N. Ichikawa and S. Uchida, *Phys. Rev. Lett.* **77**, 5417 (1996).
- ³³ K. Yoshida, A.I. Rykov, S. Tajima and I. Terasaki, *Phys. Rev. B* **60**, R15035 (1999).
- ³⁴ V.J. Emery and S.A. Kivelson, *Phys. Rev. Lett.* **74**, 3253 (1995).
- ³⁵ A.W. Tyler, A.P. Mackenzie, S. NishiZaki and Y. Maeno, *Phys. Rev. B* **58**, R10107 (1998).
- ³⁶ A.P. Mackenzie, S.R. Julian, A.J. Diver, G.J. McMullan, M.P. Ray, G.G. Lonzarich, Y. Maeno, S. Nishizaki and T. Fujita, *Phys. Rev. Lett.* **76**, 3786 (1996).
- ³⁷ A.V. Puchkov, D.N. Basov and T. Timusk, *J. Phys: Cond. Mat.* **8**, 10049 (1996).
- ³⁸ A. Goldoni, L. Sangaletti, F. Parmigiani, G. Comelli and G. Paolucci, *Phys. Rev. Lett.* **87**, 076401 (2001).
- ³⁹ J.L. Tallon, C. Bernhard, H. Shaked, R.L. Hitterman, and J.D. Jorgensen, *Phys. Rev. B* **51**, 12911 (1995).
- ⁴⁰ A.P. Mackenzie, S.R. Julian, D.C. Sinclair and C.T. Lin, *Phys. Rev. B* **53**, 5848 (1996).
- ⁴¹ R.C. Yu, M.B. Salamon, J.P. Lu and W.C. Lee, *Phys. Rev. Lett.* **69**, 1431 (1992).
- ⁴² D.A. Bonn, Ruixing Liang, T.M. Riseman, D.J. Baar, D.C. Morgan, Kuan Zhang, P. Dosanjh, T.L. Duty, A. MacFarlane, G.D. Morris, J.H. Brewer, W.N. Hardy, C. Kallin and A. J. Berlinsky, *Phys. Rev. B* **47**, 11314 (1993).
- ⁴³ H.F. He, P. Bourges, Y. Sidis, C. Ulrich, L.P. Regnault, S. Pailhes, N.S. Berzigiarova, N.N. Kolesnikov and B. Keimer, *Science* **295**, 1045 (2002).
- ⁴⁴ H.F. Fong, P. Bourges, Y. Sidis, L.P. Regnault, A. Ivanov, G.D. Guk, N. Koshizuka and B. Keimer, *Nature* **398**, 588 (1999).